



# Controllable phase formation and physical properties of yttrium oxide films governed by substrate heating and bias voltage

Pei Lei<sup>a</sup>, Bing Dai<sup>a</sup>, Jiaqi Zhu<sup>a,\*</sup>, Xiaoting Chen<sup>b</sup>, Gang Liu<sup>c</sup>, Yuankun Zhu<sup>d</sup>, Jiecai Han<sup>a</sup>

<sup>a</sup>Center for Composite Materials, Harbin Institute of Technology, P. O. Box 3010, Yikuang Street 2, Harbin 150080, PR China

<sup>b</sup>Key Laboratory for Liquid-Solid Structural Evolution and Processing of Materials (Ministry of Education), School of Materials Science and Engineering, Shandong University, Jingshi Road 17923, Jinan 250061, PR China

<sup>c</sup>Center for High Pressure Science and Technology Advanced Research, Shanghai 201203, PR China

<sup>d</sup>School of Materials Science and Engineering, University of Shanghai for Science & Technology, Shanghai 200093, PR China

HPSTAR  
0105-2015

Received 10 January 2015; received in revised form 4 March 2015; accepted 23 March 2015

Available online 1 April 2015

## Abstract

In order to understand the growth behavior of yttrium oxide films driven by thermodynamics and kinetics, two fundamental growth parameters, substrate heating and biasing, were investigated to control film structure and properties comprehensively. We observed two distinct areas, normal deposition area (area 1) and abnormal deposition area (etching area, area 2) at different substrate bias voltages regardless of the substrate temperature. X-ray diffraction (XRD) results show that heating promotes cubic phase formation, whereas ion bombardment induces monoclinic phase growth. Atomic force microscopy (AFM) measurements exhibit that the ions slightly enlarge the surface islands in area 1, whereas they flatten and smoothen the surface in area 2. X-ray photoelectron spectroscopy (XPS) results demonstrate that high temperature suppresses the physisorbed oxygen, and the ion bombardment favorably selects oxygen etching in area 1, causing excess oxygen vacancies. This selectivity almost disappears in area 2. Furthermore, the refractive index and band gap can be enhanced by both substrate temperature and bias voltage. The surface wettability of films can be modulated by the surface chemical composition.

© 2015 Elsevier Ltd and Techna Group S.r.l. All rights reserved.

**Keywords:** C. Optical properties; Y<sub>2</sub>O<sub>3</sub> film; Magnetron sputtering; Structure; Wettability

## 1. Introduction

Yttrium oxide, both a rare-earth oxide and a transition oxide, is a theoretically interesting and technologically useful material. Numerous studies have reported that yttrium oxide films can be used in a wide variety of scientific and engineering applications due to their natural properties. They include high crystallographic stability (up to 2325 °C) [1,2], superior mechanical strength [3], high permittivity (~14–18) [4,5], high refractive index (~2) [6,7], wide band gap (~5.8 eV) [8], low lattice mismatch with silicon (cubic phase) [9] and graphene (hexagonal phase) [10], well-known host matrix for rare-earth ions [11,12], and a component of several complex materials [13,14].

Similar to other rare-earth oxides, yttrium oxide has several crystallographic structures [2]. Among these crystal structures, cubic one is the most stable phase in atmospheric temperature and pressure, while other phases need much harsher conditions, i.e. high temperature and high pressure [15]. Thus, compared with other phases, cubic yttrium oxide can be easily obtained under common conditions.

Up to now, yttrium oxide films have been prepared by various methods, including molecular beam epitaxy (MBE) [16,17], pulsed laser deposition (PLD) [8,18], sputtering [7,19,20], electron beam deposition [21] etc. Most reports synthesized the cubic phase, while just a few papers reported the successful formation of other phases of yttrium oxide films. Taking monoclinic phase as an example, monoclinic yttrium oxide can be only obtained by certain conditions. Studies have shown that monoclinic yttrium oxide films have been prepared

\*Corresponding author. Tel./fax: +86 451 86417970.

E-mail address: [zhujq@hit.edu.cn](mailto:zhujq@hit.edu.cn) (J. Zhu).

by Chang et al. by MBE [16], by Lacroix through ion beam deposition [20] and by Gaboriaud with ion irradiation [22]. Similar results have also been observed for erbium oxide [23,24]. Indeed, monoclinic phase is a thermodynamically metastable phase, whose formation deviates from equilibrium. Recently, understanding and controlling the formation of cubic and/or monoclinic phases of yttrium oxide film have been the critical issues for its research and application.

Naturally, the microstructure and properties of as-deposited films can be governed by a competition process between thermodynamics and kinetics [25], which directly links to the heating and ion bombardment. These two approaches can influence the film growth processes through different ways and accordingly determine the final structures and properties. Although numerous studies have been conducted to understand the growth and properties of yttrium oxide films, the controllable phase formation and properties of yttrium oxide films under the combined substrate temperature and bias voltage are still not clear. Furthermore, it requires large work to explore the growth phase diagram and the desirable properties of yttrium oxide films under the favorable conditions for further application.

In this paper, based on above background, several groups of yttrium oxide films were prepared by magnetron sputtering under the designed conditions. The controllable growth behavior of yttrium oxide films under different substrate temperatures and bias voltages was investigated. Furthermore, the evolution of deposition rate, microstructure, optical and wettability properties was studied and discussed.

## 2. Experimental details

### 2.1. Film growth

A series of yttrium oxide films were grown on p-type silicon wafers ( $1 \times 1 \text{ cm}^2$ ) by radio frequency magnetron sputtering. Metal yttrium target with the purity of 99.999% was used as the target. Argon (99.995% purity) and oxygen gas (99.995% purity) were employed as background and reactive gas respectively. The distance between the substrate and target was 70 mm. Before the deposition, the substrates were cleaned with alcohol and acetone in an ultrasonic bath for around 30 min. During deposition, three groups of samples were prepared under three different substrate temperatures (25 °C (RT), 200 °C and 600 °C). For each group, the substrate bias voltage varied from 0 V to  $-320 \text{ V}$ . For all samples, sputtering power of 130 W and work pressure of 1.0 Pa were employed. The deposition time was two hours for all the samples to study the microstructure, morphology, chemical composition, optical constant and wettability properties. Another special group of about 500 nm yttrium oxide films was deposited on the quartz substrate for UV transmittance and optical band gap.

### 2.2. Film characterization

The crystalline structure of the films was determined by glancing incident X-ray diffraction (GIXRD, Philips X'pert) with Cu K $\alpha$  source (40 kV, 30 mA). The surface composition was detected by X-ray photoelectron spectroscopy (XPS,

Thermo ESCALAB 250) using a monochromatized Al K $\alpha$  source with a step size of 0.1 eV. No argon sputtering for XPS measurement was to avoid the surface damage by ions interaction and to keep the initial fingerprint. The binding energy of the XPS spectra was calibrated using the C1s binding energy ( $\sim 284.6 \text{ eV}$ ) of adventitious carbon. Atomic force microscope (AFM, Bruker dimension icon) was used to measure the surface morphology in contact mode at atmospheric temperature and pressure. Spectroscopic Ellipsometer (SE) was employed to investigate the optical properties in the range of 380–800 nm at the incident angle of 70°. The ultraviolet–visible spectrophotometer was used to measure the transmittance spectra of films on quartz in the range of 190–1000 nm. As for the evaluation of film wettability, the contact angles on yttrium oxide surface were measured by using a dataphysics OCA20 with a 4  $\mu\text{l}$  water and glycol.

## 3. Results and discussion

### 3.1. Film deposition rate

The deposition thickness under different growth conditions was measured by SE; the results are shown in Fig. 1. It is clear that there are two obvious areas, the large thickness ( $\sim 130 \text{ nm}$ ) in area 1, and the small thickness (below 30 nm) in area 2. In this work, heating seems to play a small role in film deposition thickness, whereas ion bombardment induced by substrate bias voltage gives a great contribution to the reduced thickness. The film surface suffers from slight ion bombardment in area 1, which has small influence on thickness. Whereas, when the negative voltage increases up to  $-240 \text{ V}$ , ions with high energy bombard the surface. In this case, the etching effect becomes dominant, removing surface adatoms and resulting in the smaller thickness compared with that in area 1. Etching plays a great role in area 2, which is consistent with the extended structure model proposed by Anders [26].

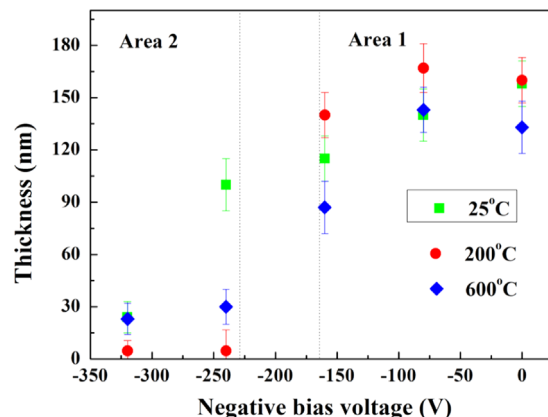


Fig. 1. The deposition thickness of films under different bias voltages and temperatures for 2 h.

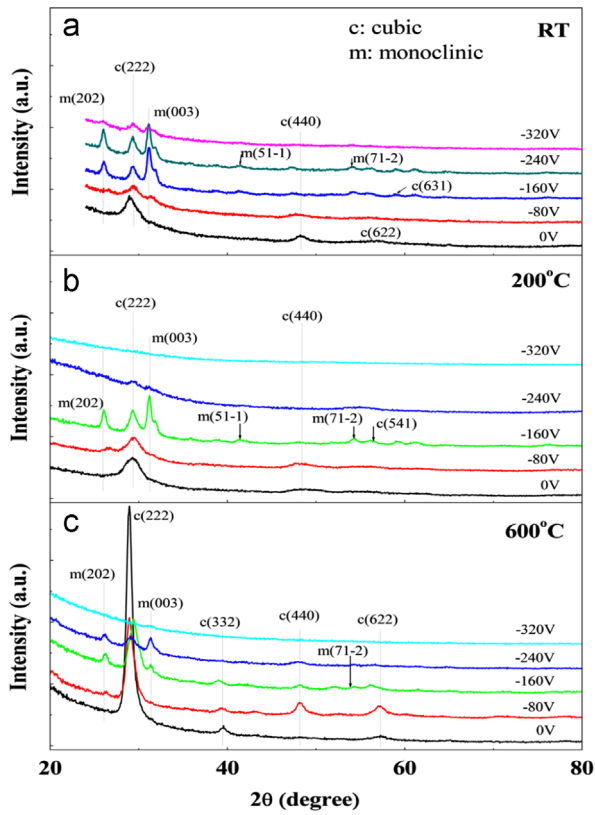


Fig. 2. GIXRD patterns of yttrium oxide films at (a) RT, (b) 200 °C and (c) 600 °C as the variation of substrate bias voltage is from 0 to -320 V.

### 3.2. Crystal structure

The XRD patterns of  $Y_2O_3$  films under different growth conditions are shown in Fig. 2. Both substrate temperature and bias voltage have great influence on the microstructures. Without bias voltage, the films show single cubic phase (ICDD file no. 00-041-1105). At low temperature, in Fig. 2(a) and (b), the films have preferential cubic (111) peak with large full width at half-maximum (FWHM). At high temperature (600 °C), films exhibit the sharp cubic (111) peak as shown in Fig. 2(c). As the biased voltage gradually increases (around  $-80$  V), besides cubic (222) peak, films show the mixture of cubic and monoclinic phases (ICDD file no. 00-044-0399) at both low and high substrate temperatures. The weak monoclinic (202) and (003) peaks as well as cubic phase peaks are observed. When the bias voltage increases to  $-160$  V, low and high temperatures demonstrate the different behaviors. The films exhibit very strong monoclinic (003) and (002) peaks mixed with weak cubic (111) peak at low temperature in Fig. 2(a) and (b). Nevertheless, the sharp and strong cubic (111) peak with several weak monoclinic (003) and (002) peaks is observed in Fig. 2(c) at high temperature. When biased voltage exceeds  $-240$  V, the peaks become very weak at both low and high substrate temperatures due to the etching effects [20,27].

Cubic phase can be easily formed at RT without bias voltage, meaning the thermodynamically stable phase. With the increase of temperature and bias voltage, films exhibit the smaller FWHM. Both heating and ion bombardment can improve the crystallinity.

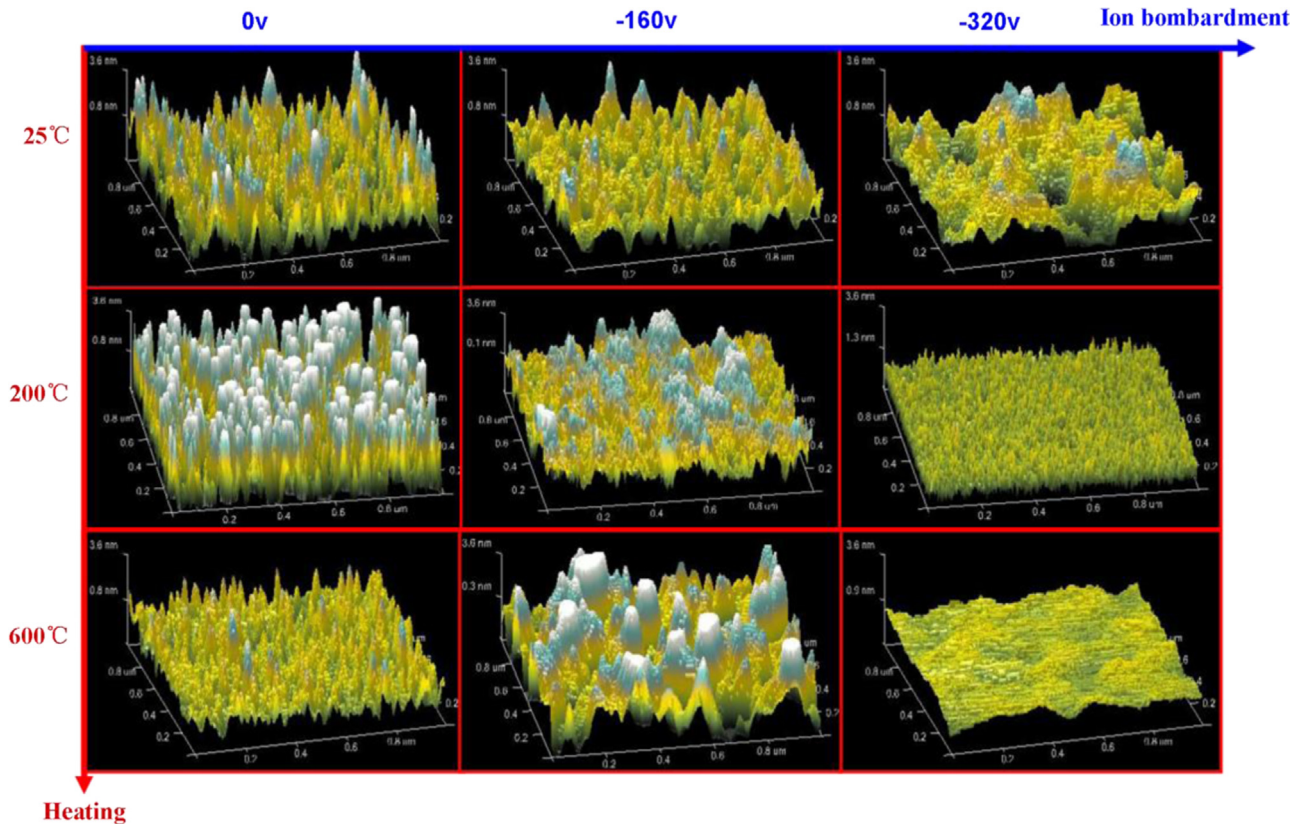


Fig. 3. AFM 3D images of yttrium oxide films at different substrate temperatures and biased voltages.

Heating can provide the adatom energy to enlarge the grains and annihilate defects. Through this way, the films prefer to form cubic phase and larger grains at high temperature. In contrast, ion bombardment promotes the adatoms' diffusion and causes dislocation by strong ions collision. These defects damage the symmetry of cubic and nucleate the monoclinic phase growth, which is also observed and reported by Gaboriaud et al. [28]. Consequently, it is reasonable to observe the dominated monoclinic phase at low temperature and cubic phase at high temperature when large biased voltage was applied on the substrate.

### 3.3. Surface morphology

AFM was employed to characterize the film surface at different growth conditions. It is clear that ion bombardment and substrate temperature have combined effects on the surface morphology evolution in Fig. 3. Although the films show different island sizes at different temperatures, without ion bombardment, the films have many uniform and sharp islands on the surface. As the biased voltage increases to  $-160$  V, the number of island decreases and several islands become large. This case is extremely obvious at  $600$  °C. When the biased voltage reaches  $-320$  V, the surface can be distinctively damaged by ion bombardment at low and high temperatures. At low temperature (RT), there exist several large islands on film surface, while the islands become more and more small and the surface is much smoother as the substrate temperature increases. Until  $600$  °C, the film surface is super-smooth and flat. Fig. 4 shows the roughness of films under the different growth conditions. Although the roughness values are floating at different substrate temperatures, the effects of ions bombardment are very clear for samples at three different temperatures. In area 1, with slight ion bombardment, the roughness value is slightly larger due to the high crystallinity [7]; whereas in area 2, as the bias voltage increases, the roughness reduces dramatically to  $\sim 0.7$  nm at RT and to the lowest value ( $\sim 0.3$  nm) at  $200$  °C and  $600$  °C, which is similar to the previous reports [29,30], corresponding well with the AFM images as shown in Fig. 3. Therefore, ion bombardment with high energy could make the surface very flat and smooth, especially at high substrate temperature.

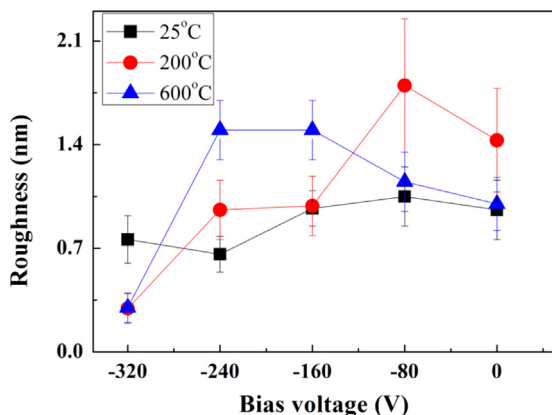


Fig. 4. The variation of surface roughness of films at  $25$  °C,  $200$  °C and  $600$  °C as a function of biased voltage.

### 3.4. Chemical composition

Fig. 5 shows the XPS spectra of O1s and Y3d of films at different growth conditions. The O1s spectra of the films at RT and at different substrate biased voltages are shown in Fig. 5(a). It is clear to observe the doublet peaks for all the films, which locate at  $529 \pm 0.1$  eV and  $531.4 \pm 0.2$  eV. They can be deconvoluted into two single peaks (Fig. 5(e)) corresponding to the O–Y [31] and  $O_\delta$  (physisorbed O or OH) [7,32]. All O1s peaks exhibit the same feature. The Y3d spectra of the films at RT display the doublet peaks with the disproportionate profiles (Fig. 5(b)). Considering the spin-splitting effects, the Y3d can be deconvoluted into two pair peaks shown in Fig. 5(f). The first pair is located at  $156.3 \pm 0.2$  eV and  $158.3 \pm 0.2$  eV, corresponding to  $Y3d_{5/2}$  and  $Y3d_{3/2}$  of Y–O bond respectively; the second one at  $158 \pm 0.2$  eV and  $160 \pm 0.2$  eV is from the  $Y3d_{5/2}$  and  $Y3d_{3/2}$  of Y–OH bond respectively [31]. The analysis for Y3d is consistent with that of O1s. At  $600$  °C, the O1s and Y3d show the similar features to those from films at RT.

The element composition was also quantified using relative sensitivity factors. The O/Y ratios are shown in Fig. 6(a) and (b) at  $25$  °C and  $600$  °C respectively. As shown in Fig. 6(a), the O/Y ratio without bias voltage is larger than the stoichiometry (1.5) at RT. As biased voltage increases to  $-160$  V, the ratio decreases monotonously to 1.27. Then, with a continual increase in the voltage, the O/Y ratio approaches to the stoichiometry. As for the O/Y ratio of films at  $600$  °C in Fig. 6(b), however, the ratio of film without bias voltage has a lower value ( $\sim 1.3$ , below stoichiometry). When the bias voltage increases, the similar trend can be observed: first decreases and then increases close to the stoichiometry. Fig. 6(c) and (d) demonstrates the O–Y/ $O_\delta$  ratios at  $25$  °C and  $600$  °C respectively. At both low and high temperatures, the O–Y/ $O_\delta$  ratio shows the similar behavior as a function of biased voltage: it first increases to  $\sim 1.25$  at  $-160$  V and then decreases to  $\sim 0.8$  at  $-320$  V.

At low temperature ( $25$  °C) and high temperature ( $600$  °C). In this work, low temperature means  $25$  °C, high temperature means  $600$  °C. In area 1, as the voltage increases, the ions have a preferential etching effect for  $O_\delta$ . Thus, the O/Y ratio decreases and the O–Y/ $O_\delta$  increases. The preferred elimination of elements was also observed in  $TiO_2$  films [33,34]. In contrast, in area 2, the ions have high energy, all the elements including O–Y and  $O_\delta$  can be removed by strong energetic ion bombardment, resulting in the ratio close to the stoichiometry. Therefore, low temperature promotes the physisorbed oxygen on the film surface, while this phenomenon can be suppressed at high temperature. In area 1, the ion bombardment prefers to eliminate the  $O_\delta$  due to the lower energy, while all the elements can be removed in area 2.

### 3.5. The schematic diagram

Fig. 7 shows the schematic diagram for the growth of yttrium oxide film under ions interaction at low and high temperatures. Without negative bias voltage, adatoms have low diffusion ability at low temperature; the condensed films always have small grains and pores at grain boundaries as shown in Fig. 7(a), which is

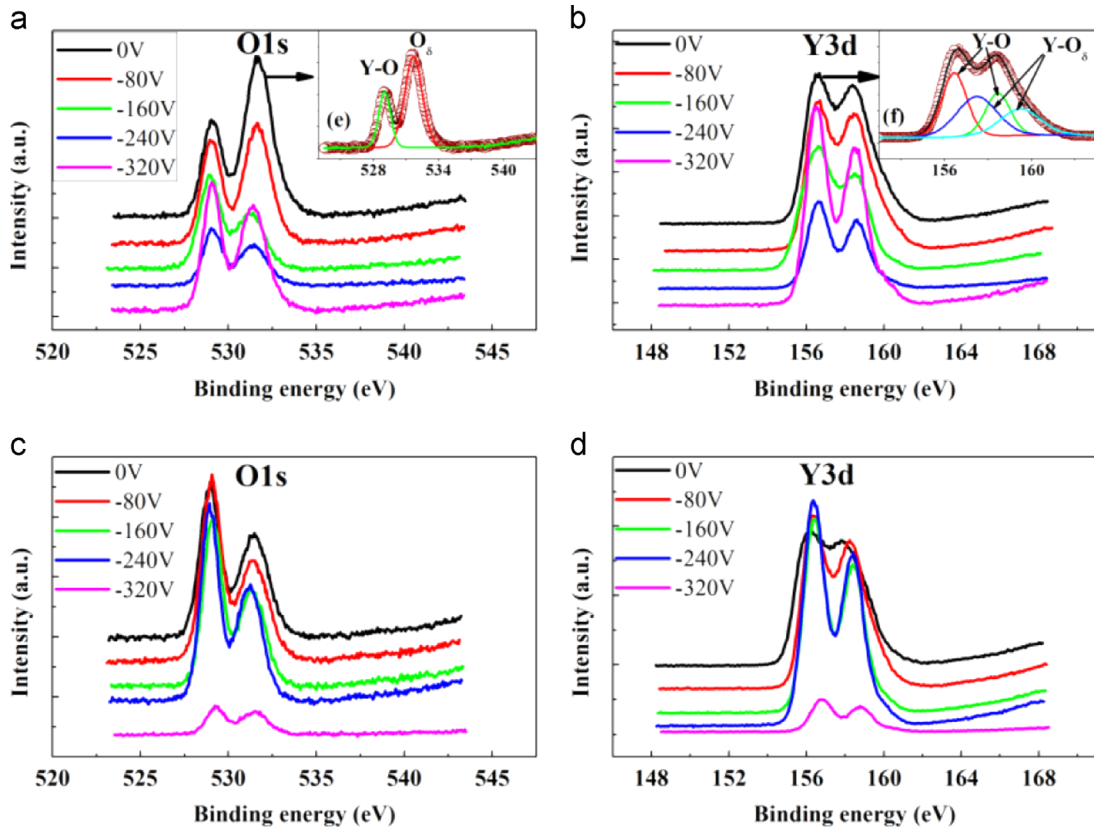


Fig. 5. XPS core level spectra of (a) O1s and (b) Y3d of films under different bias voltages at RT; (c) O1s and (d) Y3d of films under different bias voltages at 600 °C. The inserted spectra of (e) O1s and (f) Y3d of films at RT without bias voltage.

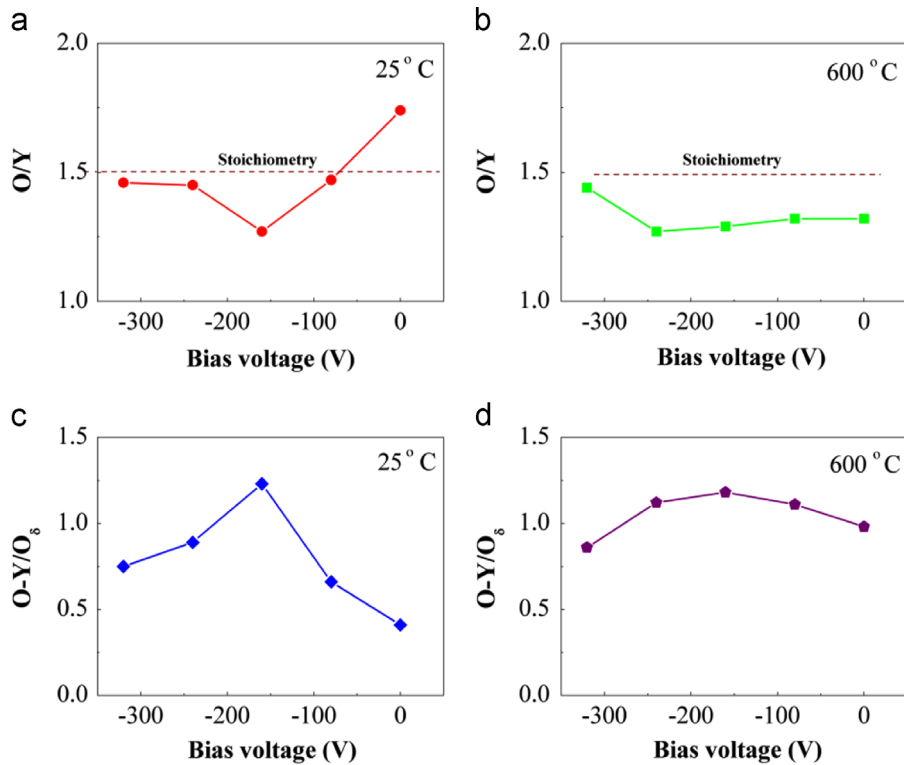


Fig. 6. The variation of O/Y ratio of films at (a) 25 °C and (b) 600 °C; the variation of O-Y/O<sub>δ</sub> ratio of films at (c) 25 °C and (d) 600 °C as a function of biased voltage.

corresponding to zone I [35]. Whereas this case is absent at high temperature, the porosity can be filled by diffused atoms due to high mobility of adatoms (Fig. 7(d)). When negative ions are applied, ions will arrive at the substrate and bombard the film surface. At  $-160$  V, the ions with high energy bombard the surface. One part of energy is delivered to the adatoms to increase the diffusion ability, and another part of energy causes a displacement cascade in the films, resulting in disordered atoms and vacancies in the film as shown in Fig. 7(b). The high temperature could relieve the damage through annihilation between interstitial atoms and vacancies. Thus, the films exhibit fewer defects at higher temperature than those at low temperature (Fig. 7(e)). The disordered oxygen vacancies are the origin of the monoclinic phase formation [28]. By increasing the voltage up to  $-320$  V, the energy is large enough to damage the surface morphology, meanwhile strongly energetic ion bombardment can remove all the elements from the surface. There still are many defects even at high temperature shown in Fig. 7(c) and (f). Generally, the thermal and kinetic factors play the competitive role in film growth. High temperature promotes the cubic nucleation and growth, while the ion bombardment tends to be the growth of defected monoclinic phase.

### 3.6. Optical properties

Optical properties were determined by SE. Three-layer model (Si substrate/SiO<sub>2</sub>/Y<sub>2</sub>O<sub>3</sub> Cauchy) was built to fit the

measured data in Fig. 8(a), and good fitting results are obtained as shown in Fig. 8(b). Because there exists etching effect and the low deposition rate in area 2, thus we only consider the optical properties of films in area 1.

The refractive indices at 550 nm of yttrium oxide films under different conditions are shown in Fig. 8(c). At point A (25 °C and no bias voltage), the film has the lowest refractive index ( $\sim 1.87$ ). There are three enhancing ways: temperature-driven way, bias voltage driven-way, and mixture of them. Through the way of temperature, the refractive index increases from point A to point B ( $\sim 1.93$ ). Combined with bias voltage driven way, the refractive index can be enhanced further to point C ( $\sim 1.96$ ). It seems that the bias voltage can give a stronger force than the role of temperature plays. Through the only voltage driven force at low temperature, the refractive index can be directly enhanced to the highest value (from point A to point C).

The enhanced mechanism can be explained distinctly under different temperatures and bias voltages. The refractive index is known to be dependent on the packing density. At point A, the film has more pore and holes and consequently has the small packing density. Since at low temperature and without bias voltage the adatoms form the holes due to the self-shadowing effects as shown in Fig. 7(a). The films can obtain high crystallinity through the way of heating and bias voltage, resulting in higher refractive indices. However, heating and bias voltage can induce different phases. Heating prefers to promote the cubic phase; while the ion bombardment induces

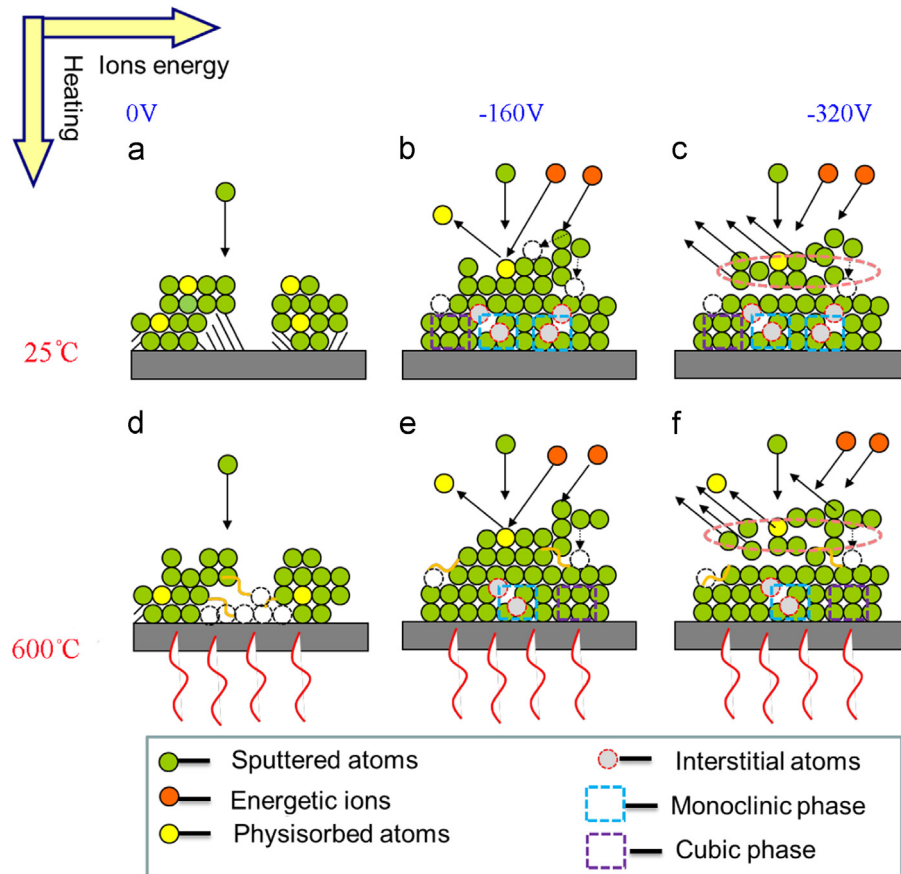


Fig. 7. The schematic diagram of films under different substrate temperatures and biased voltages.

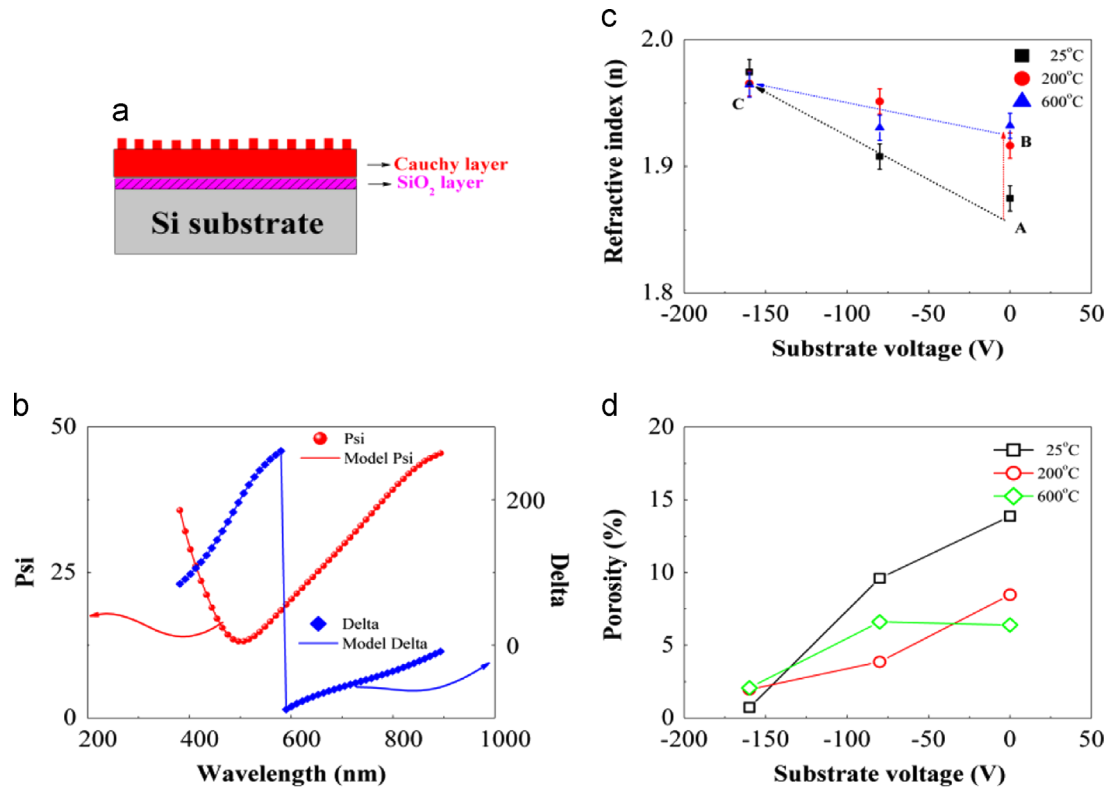


Fig. 8. (a) The built model; (b) the fitting results of films; (c) the refractive indices and (d) the porosity of films under different substrate temperatures and bias voltages.

the monoclinic phase formation in Fig. 7(b) and (e). From point A to B, the larger cubic grains play the main role in the  $n$  enhancement. Whereas from point B to C, the phase transformation from cubic to monoclinic phase is the main reason due to the larger packing density of monoclinic one (calculated density of  $5.95 \text{ g/cm}^3$ ) than that of cubic one (calculated density of  $5.03 \text{ g/cm}^3$ ). From point A goes to C, both the grain size and the crystallographic phase contribute the highest  $n$  value. Therefore, the films display the different  $n$  values under different growth conditions.

Refractive index  $n$  is linked to the relative porosity compared with that of bulk one. The volume fraction of porosity  $p$  can be extracted from the formula with the film refractive index  $n_f$  and the bulk one  $n_b$  [36]:

$$p = 1 - (n_f^2 - 1)/(n_b^2 - 1) \quad (1)$$

The calculated porosity is shown in Fig. 8(d), the porosity of film follows the reverse tendency with the variation of  $n$  value at different conditions since high refractive value corresponds to low porosity.

Yttrium oxide films ( $\sim 500 \text{ nm}$ ) were grown on quartz substrate for optical transmittance measurement. Fig. 9(a) and (b) shows the UV–visible transmittance of yttrium oxide films on quartz as a function of bias voltage and temperature. The transmittance of bare quartz is as high as 90%, while the films on quartz reduce the transmittance due to the increased reflectivity. All the films show the similar transmittance spectra with different wave lines, which is determined by the refractive index and thickness of both the film and substrate based on optical interference theory. Note that the absorption edge shifts to the

shorter wavelength, called blue-shift phenomenon, as the temperature and bias voltage increases. Using the film thickness  $t$  and transmittance  $T$ , the absorption coefficient  $\alpha$  of films can be derived from the following expression:

$$\alpha = -(1/t) \ln T \quad (2)$$

The optical band gap  $E_g$  can be estimated from the following formula using the Tauc plot:

$$ahv = A(hv - E_g)^2 \quad (3)$$

The band gap  $E_g$  can be extracted from the extrapolation of the straight line portion to the energy axis at  $\alpha=0$ . As shown in Fig. 9(c) and (d), the band gap increases with temperature and bias voltage from 5.77 eV to 6.0 eV and 5.95 eV respectively. The blueshift of band gap with the increase of temperature and bias voltage can be attributed to the increase of crystallinity [37]. Film at low temperature and no bias voltage could almost form amorphous state and very small grains, and numerous defects exist in grain boundary. These defects are able to capture electrons and holes to form the presence of unoccupied states, which is located within the forbidden area, causing the shrinkage of the band gap. When the temperature and bias voltage were applied, adatoms could move to the most suitable location, relieving defects to some extent. The more blue-shift (6.0 eV) is obtained under high temperature than that of bias voltage (5.95 eV), which can be associated with the more oxygen vacancies in monoclinic phase as electron and hole traps [38].

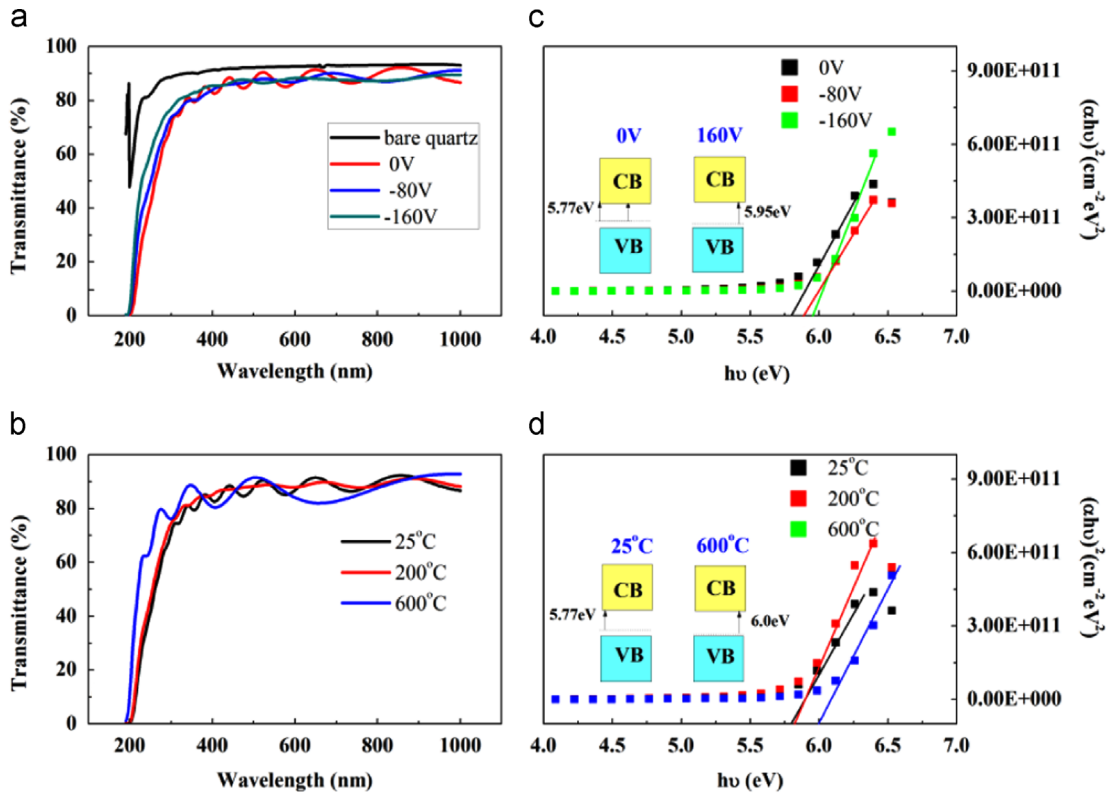


Fig. 9. The variation of transmittance of films at (a) 25 °C as a function of bias voltage and (b) 0 V as a function of substrate temperature; the variation of band gap of yttrium oxide films at (c) 25 °C as a function of bias voltage and (d) 0 V as a function of substrate temperature. The schematic of the modified band structure by bias voltage and substrate temperature were inserted.

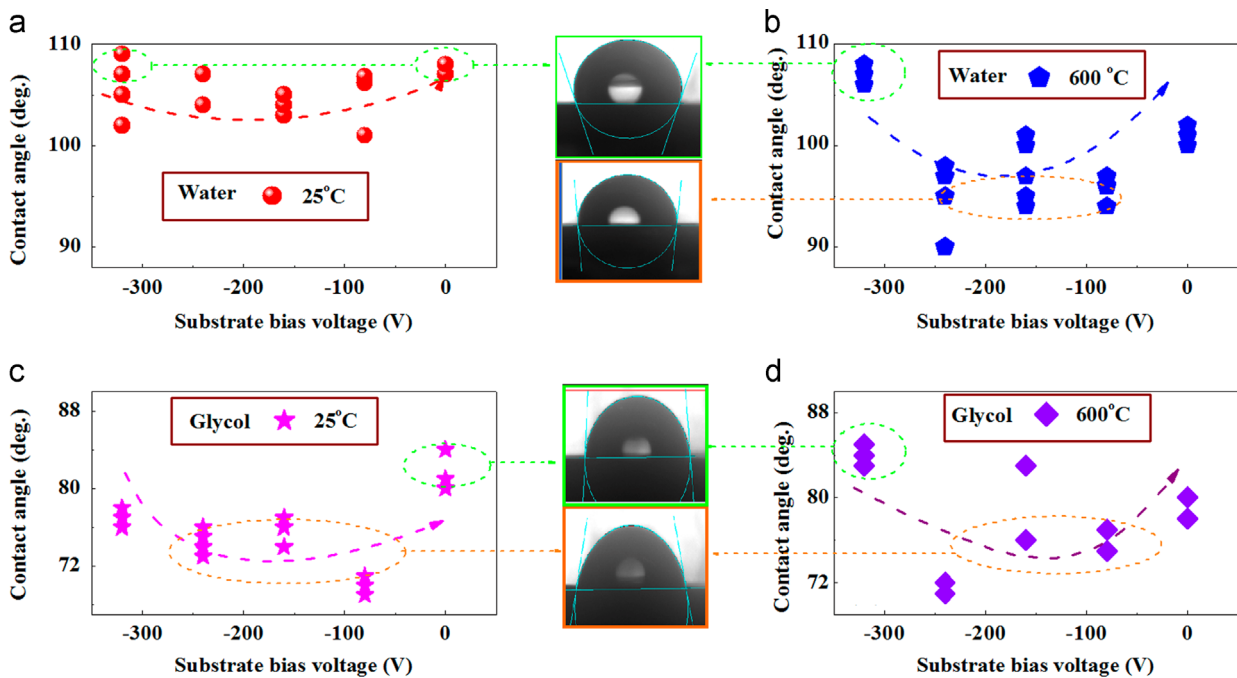


Fig. 10. The contact angles of water and glycol on yttrium oxide films' surface at (a) 25 °C and (b) 600 °C when different substrate bias voltages are applied; the contact angles of glycol on yttrium oxide surface at (a) 25 °C and (b) 600 °C when applying different substrate bias voltages.

### 3.7. Wettability

The surface properties can be modified by substrate temperature and bias voltage. In order to determine the surface

wettability, the contact angle of water and glycol on the surface was measured as shown in Fig. 10. In this work, all the samples are found to be hydrophobic for water and hydrophilic for glycol, which is consistent with the previous report [39].

Generally, the wettability of a solid surface can be controlled by a combination of the surface chemical characteristics and morphology. The effects of roughness can be explained by Wenzel's equation [40]. If the contact angle on a smooth surface is lower than  $90^\circ$ , larger roughness will reduce the contact angle, but if it is higher than  $90^\circ$ , larger roughness will further increase the contact angle. At RT and no applied bias voltage, the contact angle of water on the film surface is as high as  $\sim 108^\circ$ . With the increase of bias voltage, the angle decreases to the minimum value of  $102^\circ$ , then it returns to the starting point. Interestingly, we observed the similar trend for glycol liquid regardless of the high and low temperature. The small difference between 0 V and  $-320$  V indicates that the influence of surface roughness can be ruled out. The lowest value of contact angle may be due to the low O/Y ratio (see Fig. 6(a) and (b)), meaning defect density (oxygen vacancy). These defect sites are more kinetically favorable for the attachment of hydroxyl group, rendering the surface energetically unstable whereby the surface becomes more hydrophilic. This phenomenon has also been observed in zinc oxide [41,42]. Therefore, small contact angle on the oxygen-deficient surface at  $-160$  V can be observed. The surface wettability is beneficial for the further in/organic-device design.

#### 4. Conclusion

Three groups of yttrium oxide films under RT,  $200^\circ\text{C}$  and  $600^\circ\text{C}$  and different substrate bias voltages (from 0 V to  $-320$  V) were prepared to understand the yttrium oxide film growth driven by thermodynamics and kinetics and to study the physical properties in detail. There exist two distinct areas, normal deposition area (area 1) and etching area (area 2). Heating promotes cubic phase formation, whereas ion bombardment induces the monoclinic phase pregnancy. The ions slightly enlarge the surface roughness in area 1, whereas they flatten and smoothen the surface in area 2. High temperature suppresses the physisorbed oxygen on the surface, and the preferred oxygen etching is observed in area 1, whereas the selectivity disappears in area 2. The film growth mechanism was proposed. The optical property can be largely enhanced by ion bombardment at low and high temperatures due to the large grains and the monoclinic phase formation. The blueshift of band gap with the high temperature and bias voltage was attributed to the relief of defects. Films with the deficient oxygen composition surface have small contact angles of water and glycol. These results will provide more insights for thin film engineering.

#### Acknowledgments

The authors would like to thank the National Natural Science Foundation of China (Nos. 51222205, 51372053, and 11402149), and the Heilongjiang Province Outstanding Youth Fund (JC201305), and the Natural Science Foundation of Shanghai (No. 14ZR1428000) for the financial support of this research.

#### References

- [1] G. Adachi, N. Imanaka, The binary rare earth oxide, *Chem. Rev.* 98 (1998) 1479–1514.
- [2] M. Zinkevich, Thermodynamics of rare earth sesquioxides, *Prog. Mater. Sci.* 52 (2007) 597–647.
- [3] S. Ukai, M. Fujiwara, Perspective of ODS alloys application in nuclear environments, *J. Nucl. Mater.* 307–311 (2002) 749–757.
- [4] S. Guha, E. Cartier, M.A. Gribelyuk, N.A. Bojarczuk, M.C. Copel, Atomic beam deposition of lanthanum- and yttrium-based oxide thin films for gate dielectrics, *Appl. Phys. Lett.* 77 (2000) 2710–2712.
- [5] D. Niu, R.W. Ashcraft, Z. Chen, S. Stemmer, G.N. Parsons, Electron energy-loss spectroscopy analysis of interface structure of yttrium oxide gate dielectrics on silicon, *Appl. Phys. Lett.* 81 (2002) 676–678.
- [6] C.V. Ramana, V.H. Mudavakkat, K. Kamala Bharathi, V.V. Atuchin L.D. Pokrovsky, V.N. Kruchinin, Enhanced optical constants of nanocrystalline yttrium oxide thin films, *Appl. Phys. Lett.* 98 (2011) 031905-1–031905-3.
- [7] P. Lei, J.Q. Zhu, Y.K. Zhu, C.Z. Jiang, X.B. Yin, Yttrium oxide thin films prepared under different oxygen-content atmosphere: microstructure and optical properties, *Appl. Phys. A* 108 (2012) 621–628.
- [8] S. Zhang, R. Xiao, Yttrium oxide films prepared by pulsed laser deposition, *J. Appl. Phys.* 83 (1998) 3842–3848.
- [9] R.J. Gaboriaud, F. Pailloux, P. Guerin, F. Paumier, Yttrium oxide thin films,  $\text{Y}_2\text{O}_3$ , grown by ion beam sputtering on Si, *J. Phys. D* 33 (2000) 2884–2889.
- [10] H. Xu, Z. Zhang, Z. Wang, S. Wang, X. Liang, L.M. Peng, Quantum capacitance limited vertical scaling of graphene field-effect transistor, *ACS Nano* 5 (2011) 2340–2347.
- [11] J. Lancok, C. Garapon, C. Martinet, J. Mugnier, R. Brenier, Influence of the PLD parameters on the crystalline phases and fluorescence of  $\text{Eu:Y}_2\text{O}_3$  planar waveguides, *Appl. Phys. A* 79 (2004) 1263–1265.
- [12] O. Pons-Y-Moll, J. Perriere, E. Millon, R.M. Defourneau, D. Defourneau, B. Vincent, A. Essahlaoui, A. Boudrioua, W. Seiler, Structural and optical properties of rare-earth-doped  $\text{Y}_2\text{O}_3$  waveguides grown by pulsed-layer deposition, *J. Appl. Phys.* 92 (2002) 4885–4890.
- [13] M. Boulouz, L. Martin, A. Boulouz, A. Boyer, Effect of the dopant content on the physical properties of  $\text{Y}_2\text{O}_3\text{-ZrO}_2$  and  $\text{CaO-ZrO}_2$  thin films produced by evaporation and sputtering techniques, *Mater. Sci. Eng. B* 67 (1999) 122–131.
- [14] E. Rauwel, C. Dubourdieu, B. Holländer, N. Rochat, F. Ducroquet M.D. Rossell, G. Van Tendeloo, B. Pelissier, Stabilization of the cubic phase of  $\text{HfO}_2$  by Y addition in films grown by metal organic chemical vapor deposition, *Appl. Phys. Lett.* 89 (2006) 012902-1–012902-3.
- [15] D. Djurovic, M. Zinkevich, F. Aldinger, Thermodynamic modeling of the yttrium–oxygen system, *Calphad* 31 (2007) 560–566.
- [16] W.H. Chang, P. Chang, W.C. Lee, T.Y. Lai, J. Kwo, C.-H. Hsu J.M. Hong, M. Hong, Epitaxial stabilization of a monoclinic phase in  $\text{Y}_2\text{O}_3$  films on *c*-plane GaN, *J. Cryst. Growth* 323 (2011) 107–110.
- [17] S.E. Webster, R. Kumaran, S. Penson, T. Tiedje, Structural analysis of thin epitaxial  $\text{Y}_2\text{O}_3$  films on sapphire, *J. Vac. Sci. Technol. B* 28 (2010) C3A20–C3A23.
- [18] A.K. Singh, T.R.G. Kutty, S. Sinha, Pulsed laser deposition of corrosion protective yttrium oxide ( $\text{Y}_2\text{O}_3$ ) coating, *J. Nucl. Mater.* 420 (2012) 374–381.
- [19] H.J. Quah, K.Y. Cheong, Effects of post-deposition annealing ambient on  $\text{Y}_2\text{O}_3$  gate deposited on silicon by RF magnetron sputtering, *J. Alloy. Compd.* 529 (2012) 73–83.
- [20] B. Lacroix, F. Paumier, R.J. Gaboriaud, Crystal defects and related stress in  $\text{Y}_2\text{O}_3$  thin films: origin, modeling, and consequence on the stability of the C-type structure, *Phys. Rev. B* 84 (2011) 014104.
- [21] T.M. Pan, C.J. Chang, High-performance poly-silicon TFTs with high-*k*  $\text{Y}_2\text{O}_3$  gate dielectrics, *Semicond. Sci. Technol.* 26 (2011) 075004.
- [22] R.J. Gaboriaud, M. Jublot, F. Paumier, B. Lacroix, Phase transformations in  $\text{Y}_2\text{O}_3$  thin films under swift Xe ions irradiation, *Nucl. Instrum. Methods Phys. Res. B* 310 (2013) 6–9.

- [23] M. Tang, P. Lu, J.A. Valdez, K.E. Sickafus, Ion-irradiation-induced phase transformation in rare earth sesquioxides ( $\text{Dy}_2\text{O}_3$ ,  $\text{Er}_2\text{O}_3$ ,  $\text{Lu}_2\text{O}_3$ ), *J. Appl. Phys.* 99 (2006) 063514-1–063514-7.
- [24] C. Adelhelm, T. Pickert, M. Balden, M. Rasinski, T. Plocinski, C. Ziebert, F. Koch, H. Maier, Monoclinic B-phase erbium sesquioxide ( $\text{Er}_2\text{O}_3$ ) thin films by filtered cathodic arc deposition, *Scr. Mater.* 61 (2009) 789–792.
- [25] Z. Zhang, M.G. Lagally, Atomic processes in the early stages of thin-film growth, *Science* 276 (1997) 377–383.
- [26] A. Anders, A structure zone diagram including plasma-based deposition and ion etching, *Thin Solid Films* 518 (2010) 4087–4090.
- [27] H. Kim, J.S. Horwitz, G. Kushto, A. Piqué, Z.H. Kafafi, C.M. Gilmore, D.B. Chrisey, Effect of film thickness on the properties of indium tin oxide thin films, *J. Appl. Phys.* 8 (2000) 6021–6025.
- [28] R.J. Gaboriaud, F. Paumier, F. Pailloux, P. Guerin,  $\text{Y}_2\text{O}_3$  thin films: internal stress and microstructure, *Mater. Sci. Eng. B* 109 (2004) 34–38.
- [29] X.L. Peng, Z.H. Barber, T.W. Clyne, Surface roughness of diamond-like carbon films prepared using various techniques, *Surf. Coat. Technol.* 138 (2001) 23–32.
- [30] J.H. Kim, K.W. Chung, Microstructure and properties of silicon nitride thin films deposited by reactive bias magnetron sputtering, *J. Appl. Phys.* 83 (1998) 5831–5839.
- [31] S. Barve, M. Deo, R. Kar, N. Sreenivasan, R. Kishore, A. Biswas, B. Bhanage, M. Rao, L.M. Gantayet, D. Patil, Microwave ECR plasma assisted MOCVD of  $\text{Y}_2\text{O}_3$  thin films using  $\text{Y}(\text{tbd})_3$  precursor and their characterization, *Plasma Process. Polym.* 8 (2011) 740–749.
- [32] J. Tao, M. Batzill, Ultrathin  $\text{Y}_2\text{O}_3$  (111) films on Pt (111) substrate, *Surf. Sci.* 605 (2011) 1826–1833.
- [33] T. Kubart, T. Nyberg, S. Berg, Modelling of low energy ion sputtering from oxide surfaces, *J. Phys. D* 43 (2010) 205204.
- [34] L.I. Vergara, I. Vaquila, J. Ferrón, Titanium oxide reduction in ion depth profiling, *Appl. Surf. Sci.* 151 (1999) 129–138.
- [35] J.A. Thornton, Influence of apparatus geometry and deposition conditions on the structure and topography of thick sputtered coatings, *J. Vac. Sci. Technol.* 11 (1974) 666–670.
- [36] X.J. Wang, L.D. Zhang, J.P. Zhang, G. He, M. Liu, L.Q. Zhu, Effects of post-deposition annealing on the structure and optical properties of  $\text{Y}_2\text{O}_3$  thin films, *Mater. Lett.* 62 (2008) 4235–4237.
- [37] S. Canulescu, K. Rechendorff, C.N. Borca, N.C. Jones, K. Bordo, J. Schou, L.P. Nielsen, S.V. Hoffmann, R. Ambat, Band gap structure modification of amorphous anodic Al oxide film by Ti-alloying, *Appl. Phys. Lett.* 104 (2014) 121910-1–121910-4.
- [38] T.V. Perevalov, O.E. Tereshenko, V.A. Gritsenko, V.A. Pustovarov A.P. Yeliseyev, C. Park, J.H. Han, C. Lee, Oxygen deficiency defects in amorphous  $\text{Al}_2\text{O}_3$ , *J. Appl. Phys.* 108 (2010) 013501-1–013501-4.
- [39] H.C. Barshilia, A. Chaudhary, P. Kumar, N.T. Manikandanath, Wettability of  $\text{Y}_2\text{O}_3$ : a relative analysis of thermally oxidized, relatively sputtered and template assisted nanostructured coatings, *Nanomaterials* 2 (2012) 65–78.
- [40] Z. Lin, G.-H. Lee, Ch.-M. Liu, In-S. Lee, Controls in wettability of  $\text{TiO}_x$  films for biomedical application, *Surf. Coat. Technol.* 205 (2010) S391–S397.
- [41] M.T.Z. Myint, N.S. Kumar, G.L. Hornyak, J. Dutta, Hydrophobic/hydrophilic switching on zinc oxide micro-textured surface, *Appl. Surf. Sci.* 264 (2013) 344–348.
- [42] J. Lü, K. Huang, X. Chen, J. Zhu, F. Meng, X. Song, Z.H. Sun, Enhanced photo-induced hydrophilicity of the sol-gel-derived  $\text{ZnO}$  thin film by Na-doping, *Appl. Surf. Sci.* 257 (2011) 2086–2090.